$$\beta(\lambda,x) - \beta(0,x) = 0(\lambda^2) \qquad \text{as } \lambda \to 0 \tag{12}$$

which implies that the integrals in (11) are finite.

Application of the Riemann-Lebegue lemma to the third integral in (11) yields

$$\int_0^\infty \frac{\beta(\lambda,x) - \beta(0,x)}{\lambda^2} \cos \alpha\lambda t d\lambda = o(1) \qquad \text{as } t \to \infty \tag{13}$$

Thus (11) can be written

$$E[\Psi(x,t)] = \frac{K\alpha t}{2} + \frac{K}{2\pi} \int_0^\infty \lambda^{-2} \left[\Phi_X(\lambda) e^{-ix\lambda} + \Phi_X(-\lambda) e^{ix\lambda} - 2 \right] d\lambda + o(1) \qquad \text{as } t \to \infty \tag{14}$$

Substitution into (14) of the definition of the characteristic function,

$$\Phi_X(\lambda) = E[e^{i\lambda X}] = \int_{-\infty}^{\infty} e^{i\lambda z} dF(z) \tag{15}$$

in which F is the distribution function associated with $X(t)$, yields

$$E[\Psi(x,t)] = \frac{K\alpha t}{2} + \frac{K}{8} \int_{-\infty}^{\infty} |x - z| dF(z) + o(1) \qquad \text{as } t \to \infty \tag{16}$$

Or, since the integral in (16) is the expected value of the integrand, (16) can be written

$$E[\Psi(x,t)] = \frac{K\alpha t}{2} + \frac{K}{8} E(|x - X(t)|) \qquad \text{as } t \to \infty \tag{17}$$

It is interesting to note that, with exception of the constant factor, the stochastic term in (17) is identical with the stochastic contribution found by Knowles for the case of the elastic beam.

For the case of a stationary normal process $X(t)$ with zero mean, the characteristic function is given by

$$\Phi_X(\lambda) = \exp(-\sigma^2\lambda^2/2) \tag{18}$$

in which σ^2 is the variance of $X(t)$. Although the integral obtained with the substitution of the characteristic function $\Phi_X(\lambda)$ into (6) cannot be explicitly expressed for all x, it is possible to evaluate this integral at the mean position of the moving twisting moment, $x = 0$. The result of such an integration is given by

$$E[\Psi(0,t)] = \frac{K\sigma}{\sqrt{2\pi}} \{(e^{-t_0^2} - 1) + 2t_0 \text{ erf } (t_0)\} \tag{19}$$

where t_0 is the dimensionless time variable

$$t_0 = \frac{\alpha t}{\sqrt{2}\,\sigma} \tag{20}$$

and where erf (t_0) is the error function of t_0, which can be represented in the form of Tricomi's expansion as

$$\text{erf } (t_0) = 1/2(\pi t_0)^{1/2} e^{-t_0^2} \sum_{n=0}^{\infty} A_n t_0^n I_{n+1/2}(2t_0) \tag{21}$$

where the A_n are coefficients determined by the truncated exponential series

$$A_n = \sum_{m=0}^{n} (-1)^m/m! \tag{22}$$

and where the Γ and I symbols denote the gamma and modified Bessel functions, respectively. It is well known, see, e.g., [2, p. 139], that the infinite series in (21) is convergent in the entire positive t_0 plane.

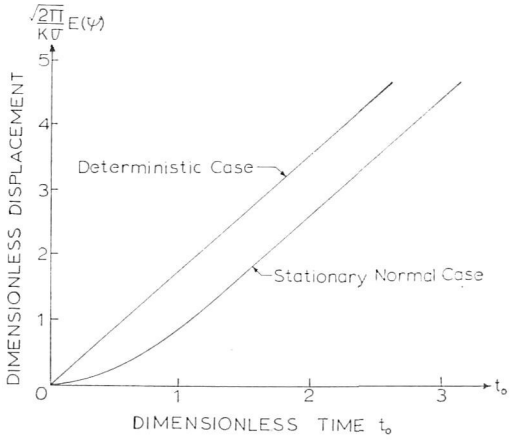

Fig. 1 Comparison of angle of twist at position of applied torque in deterministic case with expected angle of twist at mean position of applied torque with motion described by a stationary normal process

In Fig. 1 are shown the behaviors, with time, of both the angle of torsion at $x = 0$ for the deterministic case and the expected value of the angle of torsion at the mean position of the twisting moment moving according to a stationary normal process.

It can easily be shown, by considering an asymptotic expression for the error function (see, e.g., [2]), that for large time the expression for $E[\Psi(0,t)]$ given by equation (19) reduces to that predicted by equation (17).

References

1 Knowles, J. K., "On the Dynamic Response of a Beam to a Randomly Moving Load," JOURNAL OF APPLIED MECHANICS, Vol. 35, No. 1, TRANS. ASME, Series E, Vol. 90, Mar. 1968, pp. 1–6.

2 Erdelyi, A., ed., *Higher Transcendental Functions*, Vol. 2, McGraw-Hill, New York, 1953.

Flow in a Two-Dimensional Channel With a Rectangular Cavity[1]

U. B. MEHTA[2] and ZALMAN LAVAN[3]

THIS study is aimed at investigating the flow in a rectangular cavity, located in the lower wall of a two-dimensional channel. The nature of the shear-driven vortex in the cavity will, in general, depend on the Reynolds number, the aspect ratio (the height-to-length ratio) of the cavity, and the flow approaching the cavity. To minimize the number of parameters, the length of the channel is taken to be infinite and the upper wall of the channel is moved with a constant velocity. The flow is assumed to be laminar, incompressible, and Newtonian and results are obtained for different aspect ratios and Reynolds numbers.

The dimensionless equations of motion, using the length of the cavity, L, and the stream function at the moving wall, ψ_m, as the

[1] This work was sponsored by NASA Grants NGR 14-004-028 and NsG 694 and was also supported in part by the U. S. Air Force under contract AF-AFOSR 1081-66.

[2] Research Assistant, Department of Mechanical and Aerospace Engineering, Illinois Institute of Technology, Chicago, Ill.

[3] Associate Professor, Department of Mechanical and Aerospace Engineering, Illinois Institute of Technology, Chicago, Ill.

Manuscript received by ASME Applied Mechanics Division, November 25, 1968; final revision, May 12, 1969.

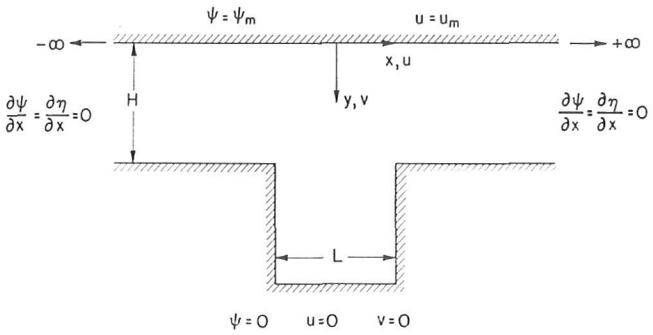

Fig. 1 Coordinate system and boundary conditions

reference dimensions, can be written in Cartesian coordinates, Fig. 1, as

$$\left(\frac{\partial^2}{\partial x^2} + \frac{\partial^2}{\partial y^2}\right)\psi = \eta, \tag{1}$$

$$\left\{\frac{\partial^2}{\partial x^2} + \frac{\partial^2}{\partial y^2} - N_{\mathrm{Re}}\left(u\frac{\partial}{\partial x} + v\frac{\partial}{\partial y}\right)\right\}\eta = 0, \tag{2}$$

where the stream function ψ is defined by

$$u = -\frac{\partial\psi}{\partial y} \qquad v = \frac{\partial\psi}{\partial x}$$

and

$$N_{\mathrm{Re}} = \frac{\psi_m}{\nu}$$

Equations (1) and (2) are transformed so that the infinite channel in the physical plane is contracted to a finite length in the transformed plane. At the same time, the transformation is chosen so that the neighborhood of each of the convex corners is expanded to facilitate the study of the rapid changes in the flow field near these points. The transformation used is

$$z = \frac{1 + \tanh a(x + 0.5)}{1 + \tanh (0.5a)} \tag{3}$$

where the value of a is determined by the number of points in the cavity for a given increment Δz. (In this study, $a = 1.386$.) This transformation, that maps $-\infty \leq x \leq 0.0$ into $0.0 \leq z \leq 1.0$, has a point of inflection at $x = -0.5$ (the upstream corner). The function is extended to the domain $0 < x \leq \infty$ by considering it antisymmetric about $z = 1.0$; i.e.,

$$1 - f(x) = f(-x) - 1$$

The transformed equations are

$$\left\{(z')^2\frac{\partial^2}{\partial z^2} + z''\frac{\partial}{\partial z} + \frac{\partial^2}{\partial y^2}\right\}\psi = \eta, \tag{4}$$

$$\left\{(z')^2\frac{\partial^2}{\partial z^2} + z''\frac{\partial}{\partial z} + \frac{\partial^2}{\partial y^2} - N_{\mathrm{Re}}\left(uz'\frac{\partial}{\partial z} + v\frac{\partial}{\partial y}\right)\right\}\eta = 0 \tag{5}$$

where primes denote differentiation with respect to x.

The entrance and exit of the channel are at an infinite distance from the cavity; therefore, it is assumed that, at these boundaries, the normal derivatives of the stream function, ψ, and vorticity, η, are zero, Fig. 1. On the remaining boundaries, the no-slip condition is applied.

Equations (4) and (5) are replaced by a system of finite-difference equations that are solved numerically using an explicit method. The numerical method, which follows the treatment of Lavan and Fejer [2],[4] is briefly described. The flow field is divided into a rectangular grid in the transformed plane and the finite-difference equations are solved for the values of the dependent variables at the nodal points. The derivatives of stream function are replaced by central differences. The second-order derivatives of vorticity are replaced by central differences and the first-order derivatives are replaced by backward or forward differences, depending on whether the coefficients of these derivatives are positive or negative. The finite-difference forms of equations (4) and (5) are

$$\psi_{i,j}^{n+1} = \psi_{i,j}^{n} + \beta_\psi\left[\frac{1}{2.0((z')^2 + c^2)} \times \left\{\psi_{i,j+1}^{n}\left((z')^2 + \frac{z''\Delta z}{2.0}\right) + \psi_{i,j-1}^{n+1}\left((z')^2 - \frac{z''\Delta z}{2.0}\right) + (\psi_{i+1,j}^{n} - \psi_{i-1,j}^{n+1})c^2 - \Delta z^2\eta_{i,j}\right\} - \psi_{i,j}^{n}\right] \tag{6}$$

$$\eta_{i,j}^{n+1} = \eta_{i,j}^{n} + \beta_\eta\left[(1.0 + c_1c_y)\eta_{i+1,j}^{n+1} + (1.0 + c_2c_y)\eta_{i-1,j}^{n} + \left\{\left(\frac{z'}{c}\right)^2 + c_4c_z\right\}\eta_{i,j+1}^{n} + \left\{\left(\frac{z'}{c}\right)^2 + c_5c_z\right\}\eta_{i,j-1}^{n+1} - \left(2.0 + 2.0\left(\frac{z'}{c}\right)^2 + (c_1 + c_2)c_y + (c_4 + c_5)c_z\right)\eta_{i,j}^{n}\right] \tag{7}$$

where i and j are defined by $z = j\Delta z$, $y = i\Delta y$, and

$$c = \frac{\Delta z}{\Delta y}, \qquad c_y = N_{\mathrm{Re}}v\Delta y, \qquad c_z = (-z'' + N_{\mathrm{Re}}z'u)\frac{\Delta y^2}{\Delta z},$$

n = level of iteration, β_ψ = overrelaxation parameter,

$$\beta_\eta = 1.0\Big/\left(2.0 + 2.0\left(\frac{z'}{c}\right)^2 + (c_1 + 2.0c_2)c_y + (2.0c_4 + c_5)c_z\right),$$

$c_1 = -1$ and $c_2 = 0$ if $c_y < 0$,

$c_1 = 0$ and $c_2 = 1$ if $c_y > 0$,

$c_4 = -1$ and $c_5 = 0$ if $c_z < 0$,

$c_4 = 0$ and $c_5 = 1$ if $c_z > 0$,

[4] Numbers in brackets designate References at end of Note.

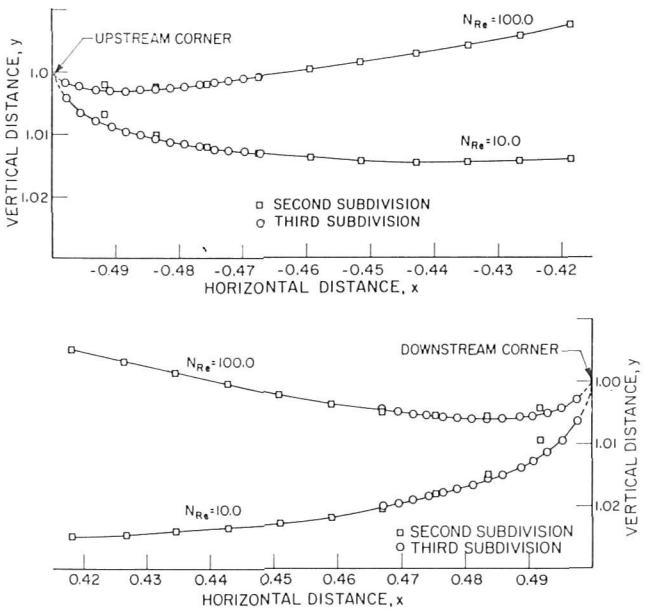

Fig. 2 Dividing streamline in immediate vicinity of convex corners

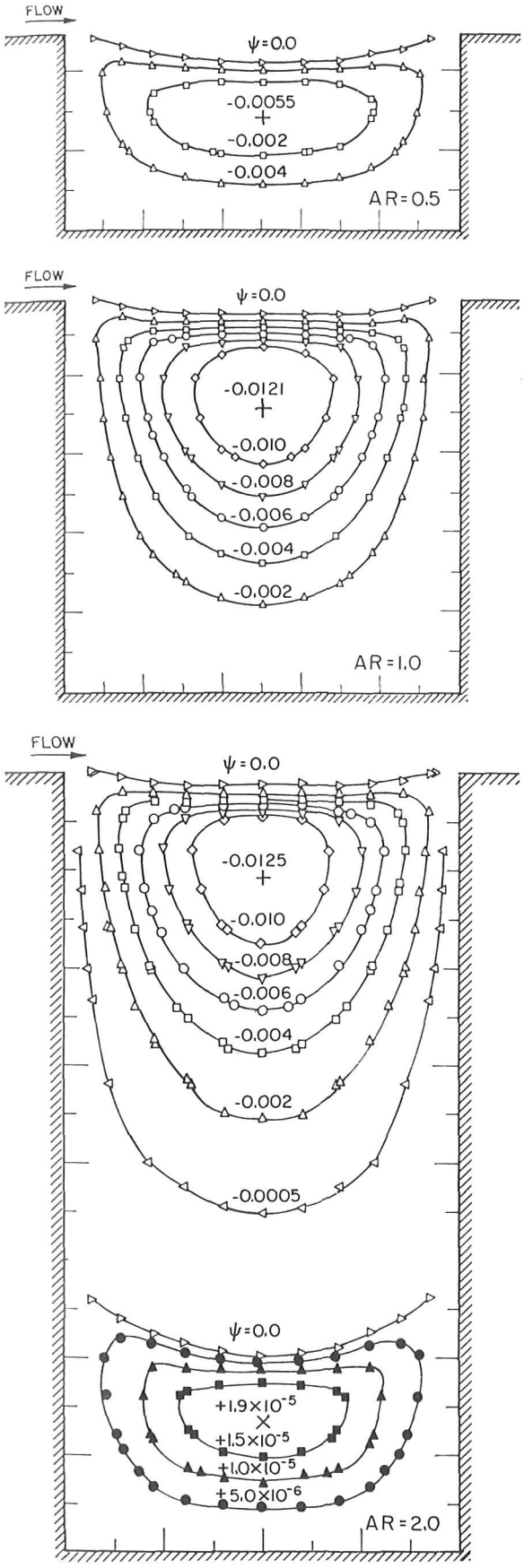

Fig. 3 Constant streamline contours at $N_{Re} = 1$

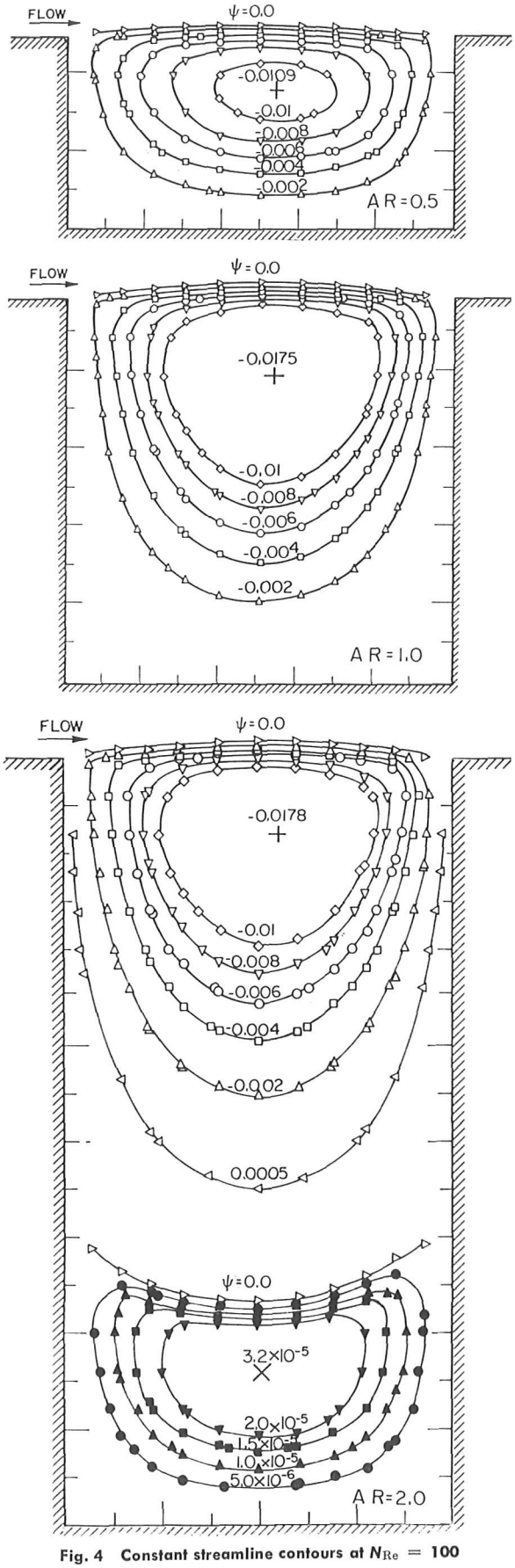

Fig. 4 Constant streamline contours at $N_{Re} = 100$

In the numerical method, the boundary conditions at the entrance and the exit are enforced by treating the boundary points as interior points and assigning reflected values to points outside the boundary. The stream function along the moving wall is equal to unity and is zero on the stationary walls. Vorticity at the solid boundaries is calculated from the stream function equation (4) subject to the no-slip condition. This is accomplished by expanding the stream function about the boundary under consideration in a Taylor series and substituting the value of the velocity at that boundary for the first derivative. Thus we get

$$\eta_w = \left(\frac{\partial^2\psi}{\partial n^2}\right)_w = (\psi^+ - \psi_w + q\Delta n)\left(\frac{2}{\Delta n^2}\right) \tag{8}$$

where ψ^+ denotes the stream function adjacent to the wall, subscript w denotes the wall, and q is the velocity of the wall under consideration. The vorticity at each of the convex corners is determined from the stream function equation evaluated at the corner, i.e.,

$$\eta_c = \left(\frac{\partial^2\psi}{\partial z^2}\right)_c + \left(\frac{\partial^2\psi}{\partial y^2}\right)_c \tag{9}$$

where c denotes the convex corner and the second derivatives are calculated using equation (8).

In all the calculations, the height of the channel, H, and the length of the cavity, L, were equal and kept constant. The solutions are determined using a grid size of 0.1 and 0.0625 in y and z-directions, respectively (resulting in a 10×11 grid inside the cavity). However, the detailed studies of the corners were carried out in the physical plane with $\Delta y = \Delta x$. The stream function and vorticity values are relaxed until the residues are smaller than 1.5×10^{-6} and 2.5×10^{-4}, respectively. Usually 150 iterations are required to achieve this accuracy and the typical time required for a single run is 13 min on an IBM 360/40/2702. Solutions were obtained for aspect ratios of 0.5, 1.0, and 2.0 and for Reynolds numbers of 1, 10, and 100.

The manner in which the dividing streamline separates and reattaches over the cavity cannot be ascertained using the 10×11 grid in the cavity. To study the flow structure in the immediate vicinity of the convex corners, a procedure similar to that followed by Pan and Acrivos [1] is used. After convergence was assured using the 10×9 grid (physical plane) in the cavity, the solution near the corners is improved by subdividing the region near each corner into finer meshes and iterating further. The boundary values of the functions for these cutaway regions are obtained by interpolating from the previous solution. This process of subdividing and solving the governing equations is repeated three times. After each subdivision, the residue limits are appropriately changed to obtain an accurate solution.

Fig. 2 shows the detailed manner of separation and reattachment of the dividing streamline in the vicinity of the convex corners for Reynolds numbers 10 and 100 as determined by the successive subdivision of the grid near these corners. This figure suggests that the dividing streamline originates at the upstream corner and terminates at the downstream corner and that it is concave near the corners. It should be noted that the present method for calculating the vorticity at the convex corners, that are singular points, gives consistent results when finer grids are used in the entire field or locally. However, when the vorticity at these points is calculated by different schemes, the position of the dividing streamline will be affected. This was also observed by Roache [4], who studied an unbounded flow over a flat plate with a square cavity.

Constant streamline plots (obtained by graphical interpolation) are shown in Figs. 3 and 4 for aspect ratios of 0.5, 1.0, and 2.0, and for Reynolds numbers of, respectively, 1 and 100. Only one vortex is observed for the aspect ratio of 1.0 and 0.5. Two vortices, one stronger than the other, are observed for a deep cavity having an aspect ratio of 2.0. The primary vortex extends to a depth of 75.0 percent and 70.9 percent of the cavity height for Reynolds numbers of, respectively, 1 and 100. This vortex has a height-to-length ratio of 1.46 at both Reynolds numbers. The numerical creeping flow solution of Pan and Acrivos [1], for the vortex flow driven by a moving surface (*prototype problem*) *with the same aspect ratio predicts this* ratio to be 1.40. An increase in the Reynolds number effects the vortex flow in the following way.

1 The strength of the vortex increases.
2 The vortex center shifts downstream and upward.
3 The streamlines in the free shear layer cluster together.
4 The streamline dividing the cavity flow and the channel flow is concave at low Reynolds numbers and convex at high Reynolds numbers (except near the corner where it is always concave).

No corner eddies were observed when the grid of 0.1×0.0625 was used. They did appear however upon local finer subdivisions. The process of subdividing and solving the governing equations was repeated up to five times. This investigation disclosed a sequence of eddies in the concave corners. Two similar vortices of decreasing strength are observed in each of the concave corners for $N_{\mathrm{Re}} = 10$ and $N_{\mathrm{Re}} = 100$. For $N_{\mathrm{Re}} = 100$, the downstream vortices are greater in size and strength than the upstream vortices and the first downstream vortex is not symmetric with respect to the diagonal of the cavity, Fig. 5. Both upstream vortices are symmetric and the ratio of the distances from the corner to the center of the first and the second vortex is 15.3. Pan and Acrivos [1] obtained this ratio to be 16.4 for the creeping flow solution of the prototype problem. For $N_{\mathrm{Re}} = 10$ (not shown here) a similar structure was observed except that in this case the downstream vortices are symmetric and almost identical to the upstream vortices. The close agreement with the prototype problem [1, 3] suggests that the flow structure in the

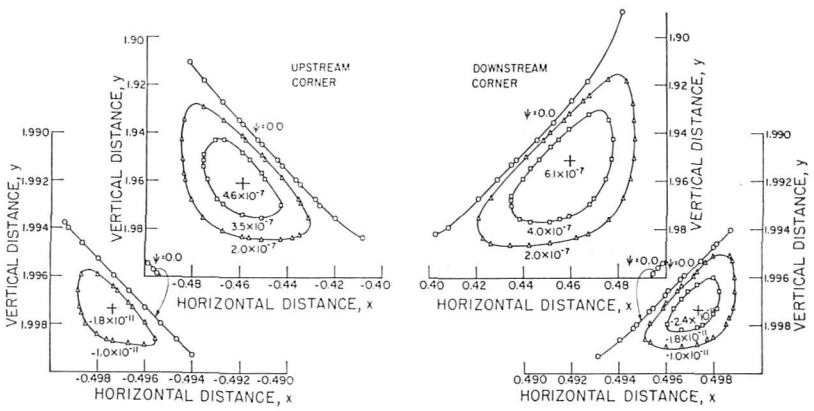

Fig. 5 Constant streamline contours for corner eddies at $N_{\mathrm{Re}} = 100$

cavity is independent of the mechanism driving the cavity flow. However, the exact location of the dividing streamline must await an analytical treatment.

References

1 Pan, F., and Acrivos, A., "Steady Flows in Rectangular Cavities," *Journal of Fluid Mechanics*, Vol. 28, 1967, pp. 643–655.

2 Lavan, Z., and Fejer, A. A., "Investigation of Swirling Flows in Ducts," ARL 66-0083, Aerospace Research Laboratories, USAF, Wright-Patterson Air Force Base, Ohio, May 1966.

3 Burggraf, O. R., "Analytical and Numerical Studies of the Structure of Steady Separated Flows," *Journal of Fluid Mechanics*, Vol. 24, 1966, pp. 113–151.

4 Roache, P. J., and Mueller, T. J., "Numerical Solutions of Compressible and Incompressible Laminar Separated Flows," AIAA Paper No. 68-741, AIAA Fluid and Plasma Dynamics Conference, June 1968.

Influence of Pressure Gradient on Turbulent Flows With Asymmetric Mean Velocity

FADEL F. ERIAN[1]

Nomenclature

x, y = space coordinates
U, V = mean velocities along x and y
u, v = fluctuating velocities along x and y
P = mean static pressure
τ = total shear stress
π = turbulent energy production
ρ, μ = density and viscosity (considered constant)

Introduction

THE statistical approach, in which fluctuating properties in a turbulent flow field are related to average values, is most useful in describing the random behavior of turbulence. In particular, expressions relating Reynolds' stress to mean velocity gradients such as those given by Boussinesq, Prandtl, von Karman, and Taylor proved to be of considerable practical value. However, all these expressions which relate the Reynolds' stress $-\rho\overline{uv}$ directly to mean flow shear $\mu(\partial U/\partial y)$ require that both shear stress modes vanish at the same locations in the flow. In turbulent flows with symmetrical mean velocity distributions this condition is met. On the other hand, in flows with asymmetric mean velocity distributions, it has been shown that the turbulent shear can no longer be conceived as being directly proportional to any power of the mean velocity gradient. Experimental evidence shows that the location in the flow where $(\partial U/\partial y) = 0$ is not the same as the location where $-\rho\overline{uv} = 0$. In this Note, the fluid zone existing between the location of zero Reynolds' stress and the location of zero mean flow shear is referred to as the "zone of opposing shear" because of the difference in sign of $-\rho\overline{uv}$ and $\mu\partial U/\partial y$.

The zone of opposing shear possesses some interesting characteristics. For instance, experiments performed in an asymmetric flow of a wall jet with zero pressure gradient [2][2] show that this zone grows in the direction of flow. Furthermore, in the zone of opposing shear the laminar shear stress opposed the action of the Reynolds' stress such that a region of minimum total shear exists [1].

[1] Assistant Professor of Mechanical Engineering, Clarkson College of Technology, Potsdam, N. Y.

[2] Numbers in brackets designate References at end of Note.

Manuscript received by ASME Applied Mechanics Division, December 18, 1968; final revision, April 17, 1969.

From an energy viewpoint, there exists a transfer of energy from the mean motion of a turbulent field to the statistical modes. This behavior is identified with the production term in the turbulent energy balance. It has been reported in the literature that a reversal in the production process exists [3] in zones of opposing shear. Since the production term is purely inertial and not a viscous phenomenon, such behavior is physically possible. Indeed, if we perform the energy balance over a control volume with solid boundaries containing a quasi-steady turbulent field, the mathematical possibility of the existence of such a region is apparent.

In this Note results of an experiment performed to study the influence of pressure gradients on the structure of turbulent shear stresses and turbulent energy production in an asymmetric flow of a wall jet are reported.

Flow Field and Apparatus

A two-dimensional, large aspect ratio wind tunnel was employed. The flow field consisted of a half jet blowing out of a narrow vertical slot, the jet being bounded by a smooth rigid flat wall on one side, and mixed with a slower stream of air on the other side. A convergent then divergent passage was provided for the entire flow by placing a half symmetrical Joukowski airfoil section on the free-stream side of the wind tunnel, Fig. 1. This airfoil section created a longitudinal pressure gradient which changed sign from negative in the convergent part to positive in the divergent part of the wind tunnel, Fig. 2.

The ratio U_j/U_s of the jet exit velocity to the free-stream velocity was maintained at the value 3.8. The free-stream velocity U_s was measured at $x = 0$, and the jet exit velocity U_j was kept at 190 fps. Two single-channel hot-wire anemometers, of the constant-temperature type, and a random signal correlator were used to measure mean velocities, turbulence intensities, and turbulent shear stress. A specially designed X-wire probe permitted measurements close to the jet wall with minimum interference. Static pressure was measured at the walls of the wind tunnel using conveniently located static pressure taps. Static pressure inside the flow was measured with a standard static pressure probe of the boundary-layer type. The wall shear stress was determined at the jet wall by a flattened Preston probe, which was carefully calibrated in a fully developed pipe flow.

Results

The quantities of interest are the total shear stress in the Reynolds' equations and the production term in the turbulent energy equation. For the complete equations, the reader is referred to [5]. In the case of two-dimensional, incompressible turbulent flow, the dominant component of shear forces is along the x-axis and is given by $\partial\tau/\partial y$, where

$$\tau = \mu \frac{\partial U}{\partial y} - \rho\overline{uv} \tag{1}$$

The turbulent energy production is given by

$$\pi = -\left[\overline{uv}\,\frac{\partial V}{\partial x} + \overline{vu}\,\frac{\partial U}{\partial y} + \overline{u^2}\,\frac{\partial U}{\partial x} + \overline{v^2}\,\frac{\partial V}{\partial y}\right]$$

It has been shown experimentally [6, 7] that the term containing $(\partial V/\partial x)$ is much smaller than the other production terms. In addition, by the condition of continuity of mean motion, we have $(\partial V/\partial y) = -(\partial U/\partial x)$. Accordingly, π may be approximated by

$$\pi = -\left[\overline{uv}\,\frac{\partial U}{\partial y} + (\overline{u^2} - \overline{v^2})\,\frac{\partial U}{\partial x}\right] \quad \text{(fps)}^3/\text{in.} \tag{2}$$

Fig. 2 shows the distributions of static pressure at the tunnel walls.

Fig. 3 shows a typical distribution of turbulent shear in the negative pressure gradient section of the flow. Fig. 4 shows a